SUPPORTING INFORMATION

Efficiency-limiting Processes in Cyclopentadithiophene-bridged Donor-Acceptor-type Dyes for Solid-State Dye-sensitized Solar Cells

Felix Hinkel,[§] Yoojin M. Kim,[§] Yulian Zagraniarsky, Florian Schlütter, Denis Andrienko, Klaus Müllen*, and Frederic Laquai*

Max-Planck-Institute for Polymer Research, Ackermannweg 10, D-55128 Mainz, Germany

King Abdullah University of Science and Technology (KAUST), KAUST Solar Center (KSC), Physical Sciences and Engineering Division (PSE), Material Science and Engineering Program (MSE), Thuwal, 23955-6900, Kingdom of Saudi Arabia

1. Methods

All used chemicals and solvents were obtained from the companies ABCR, Acros, Aldrich, Alpha-Aesar, Fluka, Lancaster, Merck and Strem. Unless otherwise mentioned, they were used as received. Oxygen or moisture sensitive reactions were carried out under inert atmosphere (Westfalen AG). If not mentioned otherwise, reactions were degassed by bubbling a stream of argon through the reaction mixture. All polymerizations were degassed using a three times freeze-pump-purge method. 1H-NMR and 13C-NMR experiments were recorded in the listed deuterated solvents on a Bruker AMX 300, Bruker DRX 500 or a Bruker DRX 700 spectrometer. The deuterated solvent was used as an internal standard. Field-desorption mass spectra were obtained on a VG Instruments ZAB 2-SE-FPD. High-resolution electrospray ionization (HR-ESI) mass spectrometry was performed at the University of Mainz on a QTof Ultima 3 spectrometer by the firm Micromass/Waters. Solution UV-vis spectra were recorded at room temperature on a Perkin-Elmer Lambda 100 spectrophotometer. The baseline was corrected by subtracting a measurement of the cuvette filled with pure solvent used for the measurement.

2. Synthesis:

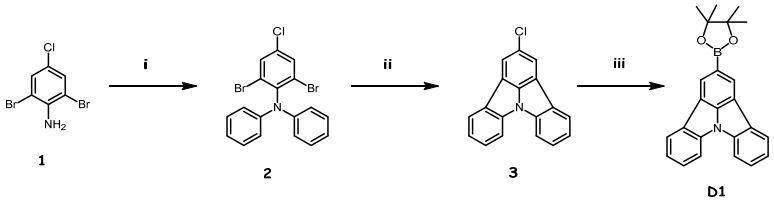

Scheme 1. i) Iodobenzene, Cu, 18-crown-6, K_2CO_3, o-xylene, reflux, 40 h. 57 % ii) $Pd(OAc)_2$, PCy_3, K_2CO_3, DMA, 90°C, 2 h, 93 % iii) 4,4,4',4',5,5,5',5'-octamethyl-2,2'-bi(1,3,2-dioxaborolane), $Pd(dba)_2$, PCy_3, KOAc, 1,4-dioxane, 95°C, 48 h, 68 %.

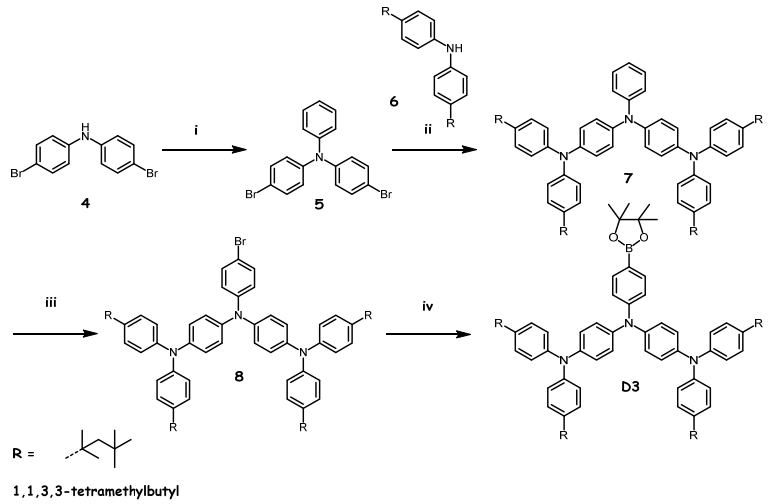

Scheme 2. i) Iodobenzene, Cu, CuI, 18-crown-6, K_2CO_3, mesitylene, 160°C, 24 h, 83 % ii) **5**, **6**, $Pd_2(dba)_3$ (5 mmol%), sodium *tert*-butylat, tri(*tert*-butyl)phosphine (10 mol%), toluene, 90°C, 2 h, 91 % iii) NBS, $CHCl_3$, rt, 20 h, 95 % iv) bis(pinacolato)diboron, $PdCl_2$(dppf), KOAc, 1,4-dioxane, 90°C, 5 h, 56 %.

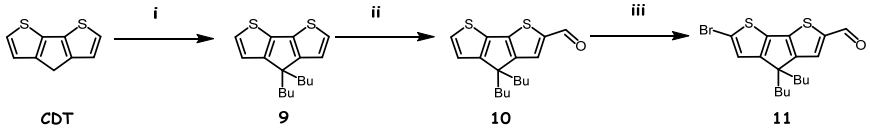

Scheme 3. i) 1-Butylbromide, KOH, KI, DMF, 50°C, 24 h, 99 % ii) *n*-BuLi, DMF, -78°C, 1 h, 70 % iii) NBS, chloroform, rt, 24 h, 98 %.

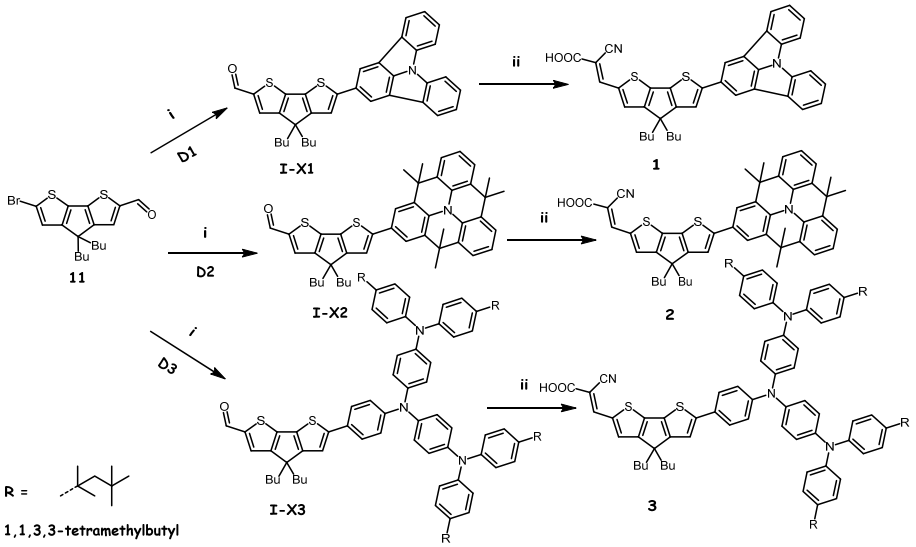

Scheme 4. i) $Pd(PPh_3)_4$, K_2CO_3, toluene, H_2O, 100°C, 24 h, 95-97 % ii) 2-cyanoacetic acid, piperidine, $CHCl_3$, 85°C, 6 h, 60 – 85 %.

4,4-Dibutyl-4*H*-cyclopenta[2,1-*b*:3,4-*b'*]dithiophene **9**

500 mg 4H-Cyclopenta[2,1-b:3,4-b']dithiophene (2.8 mmol), 456 mg 1-bromobutane (8.0 mmol) and 3 mg potassium iodide (0.02 mmol) were dissolved in 35 mL DMF. Subsequently, 560 mg potassium hydroxid (10 mmol) were added and the reaction was stirred at 50 °C overnight. After extraction with DCM, the crude product was purified by column chromatography (hexane). The product was obtained as colorless oil in 99 % yield (814 mg, 2.8 mmol). MS (FD, 8 kV): m/z (%) = 290.1 (100) (berechnet für C17H22S2 = 290.1). ESI-HR MS: berechnet für C17H23S2 ([M+H+]) 291.1241, found 291.1242. 1H NMR (300 MHz, CD2Cl2): δ = 7.03 (d, J = 4.9 Hz, 2H), 6.87 (d, J = 4.9, 2H), 1.90 (td, J = 6.7, 2.6 Hz, 4H), 1.17 (dd, J = 14.7, 7.3 Hz, 4H), 1.04 – 0.84 (m, 4H), 0.76 (t, J = 7.3 Hz, 6H). 13C NMR (75 MHz, CD2Cl2): δ = 156.73, 134.81, 122.89, 120.14, 54.36, 37.95, 27.27, 23.55, 14.22.

4,4-Dibutyl-4*H*-cyclopenta[1,2-*b*:5,4-*b'*]dithiophene-2-carbaldehyde **10**

1.75 mL n-BuLi (2.8 mmol) were added to a solution of 800 mg 4,4-dibutyl-4H-cyclopenta[2,1-b:3,4-b']dithiophene (2.74 mmol) in dry THF (20 mL) at -78 °C. The solution was stirred for 30 min, when 0.4 mL DMF (365 mg, 5 mmol) were added. After completion of the reaction, extraction with DCM and column chromatography (hexane: DCM v:v = 2:1) yielded 604 mg (1.9 mmol, 70 %) of the desired product as pale yellow oil. MS (FD, 8 kV): m/z (%) = 318.2 (100) (calcd. C18H22OS2 = 318.1). ESI-HR MS: calcd. C18H23OS2 ([M+H+]) 319.1190, found 319.1193. 1H NMR (300 MHz, CD2Cl2): δ = 9.82 (s, 1H), 7.61 (s, 1H), 7.43 (d, J = 4.9 Hz, 1H), 7.03 (d, J = 4.9 Hz, 1H), 1.90 (td, J = 6.7, 2.6 Hz, 4H), 1.17 (dd, J = 14.7, 7.3 Hz, 4H), 1.04 – 0.84 (m, 4H), 0.76 (t, J = 7.3 Hz, 6H). 13C NMR (75 MHz, CD2Cl2): δ = 183.06, 163.10, 158.81, 147.85, 143.85, 136.11, 130.92, 130.09, 122.52, 54.36, 37.95, 27.27, 23.55, 14.22.

6-Bromo-4,4-dibutyl-4*H*-cyclopenta[1,2-*b*:5,4-*b'*]dithiophene-2-carbaldehyde **11**

To a solution of 580 mg 4,4-dibutyl-4H-cyclopenta[1,2-b:5,4-b']dithiophene-2-carbaldehyd (1.8 mmol) in 20 mL dry DMF were added 356 mg NBS (2.0 mmol) at 0 °C and the reaction was stirred for 24 h. Water (100 mL) was added and the product was extracted 3 times in 100 mL DCM. The solvent was

removed and the crude product was purified by column chromatography (hexane: DCM v:v = 2:1, Rf = 0.6) yielding a yellow solid. (698 mg, 1.76 mmol, 98 %).

MS (FD, 8 kV): m/z (%) = 396.0 (100) (calcd. C18H21BrOS2 = 396.0). ESI-HR MS: calcd. C18H22BrOS2 ([M+H+]) 397.0295, found 397.0300. 1H NMR (300 MHz, CD2Cl2): δ = 9.81 (s, 1H), 7.58 (s, 1H), 7.05 (s, 1H), 2.02 – 1.68 (m, 4H), 1.16 (m, 4H), 0.88 (m, 4H), 0.76 (t, J = 7.3 Hz, 6H). 13C NMR (75 MHz, CD2Cl2): δ = 183.10, 161.70, 157.91, 146.92, 144.28, 136.61, 130.63, 125.73, 116.44, 55.20, 37.87, 27.21, 23.52, 14.19.

4,4-Dibutyl-6-(indolo[3,2,1-*jk*]carbazol-2-yl)-4*H*-cyclopenta[1,2-*b*:5,4-*b'*]dithiophene-2-carbaldehyde **I-X1**

200 mg 6-Bromo-4,4-dibutyl-4*H*-cyclopenta[1,2-*b*:5,4-*b'*]dithiophene-2-carbaldehyde (0.5 mmol), 202 mg 2-(4,4,5,5-tetramethyl-1,3,2-dioxaborolan-2-yl)indolo[3,2,1-*jk*]carbazol (0.55 mmol), 207 mg potassium carbonate (1.5 mmol) and 57 mg tetrakis(triphenylphosphin)palladium (0.05 mmol) were dissolved in 5 mL toluene and 1 mL water and stirred at 100°C over night. Water was added and the product was extracted in DCM. After removal of the solvent, column chromatography (hexane, DCM v:v = 1:1, Rf = 0.4) yielded an orange solid (267 mg, 0.48 mmol, 96 %).

MS (FD, 8 kV): m/z (%) = 557.2 (100) (calcd. C36H31NOS2 = 557.2). ESI-HR MS: calcd. C36H32NOS2 ([M+H+]) 558.1925, found 558.1930. 1H-NMR (CH2Cl2, 300 MHz): δ = 9.82 (s, 1H), 8.36 (s, 2H), 8.20 (d, J = 7.4 Hz, 2H), 7.94 (d, J = 8.1 Hz, 2H), 7.69 – 7.51 (m, 3H), 7.51 – 7.30 (m, 3H), 2.08 – 1.90 (m, 4H), 1.31 – 1.11 (m, 4H), 1.10 – 0.95 (m, 4H), 0.93 – 0.68 (m, 6H). 13C-NMR (CH2Cl2, 300 MHz): δ = 182.53, 163.89, 157.83, 151.82, 149.04, 148.87, 148.13, 143.18, 139.66, 134.42, 130.81, 130.52, 130.09, 127.76, 123.77, 122.51, 119.23, 118.19, 112.85, 54.63, 37.94, 27.19, 23.46, 14.08.

4,4-Dibutyl-6-(4,4,8,8,12,12-hexamethyl-8,12-dihydro-4*H*-benzo[1,9]quinolizino[3,4,5,6,7-*defg*]acridin-2-yl)-4*H*-cyclopenta[1,2-b:5,4-b']dithiophene-2-carbaldehyde **I-X2**

According to the procedure for **I-X1**, 200 mg 6-bromo-4,4-dibutyl-4*H*-cyclopenta[1,2-*b*:5,4-*b'*]dithiophene-2-carbaldehyd (0.5 mmol), 270 mg 4,4,8,8,12,12-hexamethyl-2-(4,4,5,5-tetramethyl-1,3,2-dioxaborolan-2-yl)-8,12-dihydro-4*H*-benzo[9,1]quinolizino[3,4,5,6,7-*defg*]acridine (0.55 mmol), 207 mg potassium carbonate (1.5 mmol) and 57 mg tetrakis(triphenylphosphin)palladium (0.05 mmol) were used. An orange solid was obtained after purification (330 mg, 0.49 mmol, 97 %).

MS (FD, 8 kV): m/z (%) = 681.4 (100) (calcd. C45H47NOS2 = 681.3). ESI-HR MS: calcd. C45H48NOS2 ([M+H+]) 682.3177, found 682.3172. 1H-NMR (CH2Cl2, 300 MHz): δ = 9.74 (s, 1H), 7.57 (s, 2H), 7.52 (s, 1H), 7.34 (dd, J = 6.9, 1.3 Hz, 4H), 7.18 (s, 1H), 7.08 (t, J = 7.7 Hz, 2H), 1.87 (dd, J = 10.3, 6.0 Hz, 4H), 1.60 (s, 12H), 1.56 (s, 6H), 1.20 – 1.04 (m, 4H), 0.90 (m, 4H), 0.79 (m, 4H), 0.74 – 0.65 (m, 6H). 13C-NMR (CH2Cl2, 300 MHz): δ = 182.60, 164.12, 157.80, 150.97, 150.08, 143.17, 133.92, 131.83, 130.90, 130.48, 130.02, 129.25, 127.05, 124.24, 123.85, 123.65, 121.07, 119.93, 116.95, 54.59, 38.06, 35.98, 33.56, 32.97, 30.07, 27.10, 23.43, 14.05.

6-(4-(Bis(4-(bis(4-(2,4,4-trimethylpentan-2-yl)phenyl)amino)phenyl)amino)phenyl)-4,4-dibutyl-4*H*-cyclopenta[2,1-*b*:3,4-*b'*]dithiophene-2-carbaldehyde **I-X3**

According to the procedure for **I-X1**, 200 mg 6-bromo-4,4-dibutyl-4*H*-cyclopenta[1,2-*b*:5,4-*b'*]dithiophene-2-carbaldehyde (0.5 mmol), 588 mg *N*1-(4-(bis(4-(2,4,4-trimethylpentan-2-

yl)phenyl)amino)phenyl)-*N*1-(4-(4,4,5,5-tetramethyl-1,3,2-dioxaborolan-2-yl)phenyl)-*N*4,*N*4-bis(4-(2,4,4-trimethylpentan-2-yl)phenyl)benzol-1,4-diamine (0.55 mmol), 207 mg potassium carbonate (1.5 mmol) and 57 mg tetrakis(triphenylphosphin)palladium (0.05 mmol) were used. An orange solid was obtained (639 mg, 0.47 mmol, 95 %).

MS (FD, 8 kV): m/z (%) = 1343.8 (100) (calcd. C92H117N3OS2 = 1343.9). ESI-HR MS: calcd. C92H118N3OS2 ([M+H+]) 1344.8716, found 1344.8722.

2-Cyano-3-(4,4-dibutyl-6-(indolo[3,2,1-*jk*]carbazol-2-yl)-4*H*-cyclopenta[2,1-*b*:3,4-*b'*]dithiophene-2-yl)acrylic acid **1**

111 mg 4,4-Dibutyl-6-(indolo[3,2,1-*jk*]carbazol-2-yl)-4*H*-cyclopenta[1,2-*b*:5,4-*b'*]dithiophen-2-carbaldehyde (0.2 mmol) were dissolved in 10 mL dry chloroform and added to a solution of 170 mg 2-cyanoacetic acid (2 mmol) in 5 mL dry ethanol. 1 mL Dry piperidine (850 mg, 10 mmol) were added and the solution was heated to 85°C in a sealed tube over night. Water was added and the product was extracted in DCM. After removal of the solvent, column chromatography with gradient from pure DCM (100 %) to DCM: Ethanol (v:v = 20:1) yielded a red solid (75 mg, 0.12 mmol, 60 %).

ESI-HR MS: calcd. C39H33N2O2S2 ([M+H+]) 625.1983, found 625.1989. 1H-NMR (CH2Cl2, 500 MHz): δ = 8.28 – 8.23 (s, 2H), 8.22 (s, 1H), 8.08 (d, J = 7.7 Hz, 2H), 7.85 (d, J = 8.0 Hz, 2H), 7.56 (s, 1H), 7.49 (t, J = 7.7 Hz, 2H), 7.40 – 7.22 (m, 3H), 1.88 (m, 4H), 1.12 (m, 4H), 0.92 (q, J = 10.1, 9.1 Hz, 4H), 0.69 (t, J = 7.3 Hz, 6H). 13C-NMR (CH2Cl2, 300 MHz): δ = 165.04, 164.81, 164.39, 164.17, 157.74, 156.60, 153.59, 152.48, 152.42, 149.11, 148.37, 146.74, 143.66, 139.05, 136.48, 135.98, 135.26, 133.96, 131.46, 130.27, 130.21, 129.46, 127.42, 123.42, 122.15, 118.67, 117.91, 117.74, 117.55, 112.55, 90.45, 67.57, 29.53, 26.73, 22.96, 13.76.

2-Cyano-3-(4,4-dibutyl-6-(4,4,8,8,12,12-hexamethyl-8,12-dihydro-4*H*-benzo[9,1]quinolizino[3,4,5,6,7-*defg*]acridin-2-yl)-4*H*-cyclopenta[2,1-*b*:3,4-*b'*]dithiophen-2-yl)acrylic acid **2**

According to the procedure for **1**, 136 mg 4,4-dibutyl-6-(4,4,8,8,12,12-hexamethyl-8,12-dihydro-4*H*-benzo[1,9]quinolizino[3,4,5,6,7-*defg*]acridin-2-yl)-4*H*-cyclopenta[1,2-*b*:5,4-*b'*]dithiophene-2-carbaldehyde (0.2 mmol), 170 mg 2-cyanoacetic acid (2 mmol) in 5 mL dry ethanol and 1 mL dry piperidine (850 mg, 10 mmol) were used. A red solid was obtained in 85 5 yield (127 mg, 0.17 mmol).

ESI-HR MS: calcd. C48H49N2O2S2 ([M+H+]) 749.3235, found 749.3241. 1H-NMR (CH2Cl2, 500 MHz): δ = 8.19 (s, J = 2.7 Hz, 1H), 7.57 (s, 2H), 7.51 (s, 1H), 7.34 (m, 4H), 7.20 (s, 1H), 7.08 (m, 2H), 1.88 (tdd, J = 15.9, 12.1, 7.2 Hz, 4H), 1.60 (s, 12H), 1.55 (s, 6H), 1.34 – 1.00 (m, 4H), 1.02 – 0.75 (m, 4H), 0.70 (td, J = 7.4, 2.8 Hz, 6H). 13C-NMR (CH2Cl2, 300 MHz): δ = 164.99, 164.21, 157.83, 157.63, 150.70, 149.32, 146.67, 146.54, 136.59, 135.94, 134.83, 133.64, 132.34, 131.35, 130.97, 130.49, 130.07, 129.69, 128.80, 127.52, 125.18, 123.86, 123.46, 123.36, 123.31, 120.68, 117.55, 116.61, 94.46, 54.59, 29.32, 26.67, 26.59, 22.99, 22.89, 22.66, 13.89, 13.62.

3-(6-(4-(Bis(4-(bis(4-(2,4,4-trimethylpentan-2-yl)phenyl)amino)phenyl)amino)phenyl)-4,4-dibutyl-4*H*-cyclopenta[2,1-*b*:3,4-*b'*]dithiophen-2-yl)-2-cyanoacrylic acid **3**

According to the procedure for **1**, 268 mg 6-(4-(bis(4-(bis(4-(2,4,4-trimethylpentan-2-yl)phenyl)amino)phenyl)amino)phenyl)-4,4-dibutyl-4*H*-cyclopenta[2,1-*b*:3,4-b']dithiophene-2-carbaldehyde (0.2 mmol), 170 mg 2-cyanoacetic acid (2 mmol) in 5 mL dry ethanol and 1 mL dry piperidine (850 mg, 10 mmol) were used. A red solid was obtained in 73 % yield (206 mg, 0.15 mmol). ESI-HR MS: calcd. C95H119N4O2S2 ([M+H+]) 1411.8774, found 1411.8783.

3. DFT calculations

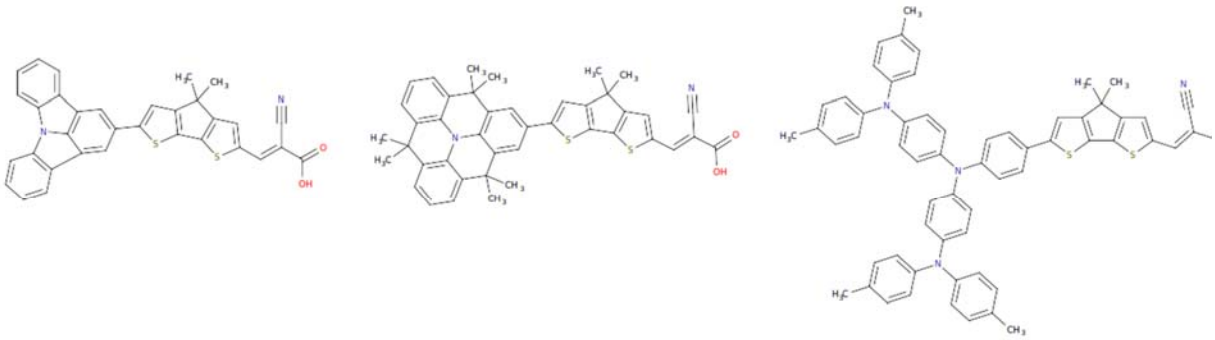

D1 D2 D3

Figure S1. The structures of three dyes which served as an input for the geometry optimization are shown in Figure S1. Some of the solubilizing groups were removed to reduce the computational effort.

Total energies of neutral and cationic forms are summarized in Table S1.

	D1	D2	D3
Neutral (Hartree)	-2326.29648853	-2678.99959621	-3521.14533410
Cation geometry, cation	-2326.06045866	-2678.77798018	-3520.94347745
Neutral geometry, cation	-2325.93011968	-2678.69017441	-3520.73365485
Dipole moment, neutral molecule, Debye	8.5987 -5.5, 0.7, 6.5	8.6127 -7.1, 0.5, -4.8	10.5392 7.6, -5.2, -5.1
Vertical IP (eV)	9.97	8.42	11.2
IP (eV)	6.42	6.03	5.49
HOMO (Hartree)	-0.20301	-0.18846	-0.17638
LUMO (Hartree)	-0.10197	-0.10207	-0.09917
S1 (neutral geometry)	2.85170 eV 434.78 nm f=0.8550	2.1335 eV 581.12 nm f=0.7557	1.8884 eV 656.56 nm f=0.5364
Dipole in the excited state, Debye	8.6 -7.0, -4.6, 1.9	8.6 -6.9, -4.9, 1,5	10.5 9.3, -2.8, -4.1

Table S1. Total energies of neutral andcationic forms

Figure S2 shows the HOMO (left) and LUMO (right) orbitals. The HOMO is delocalized over the entire molecule, while LUMO is localized on the acceptor end of the molecule.

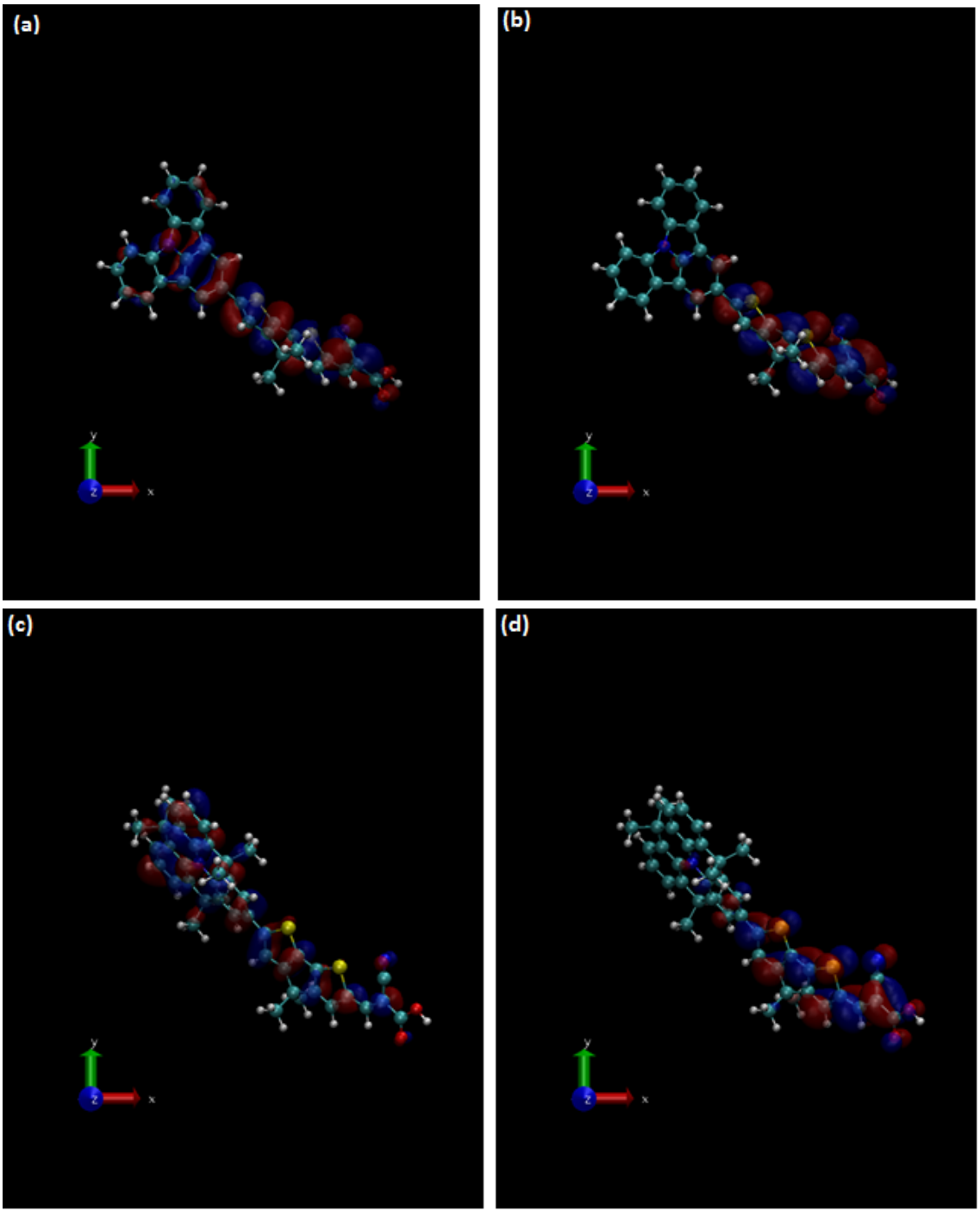

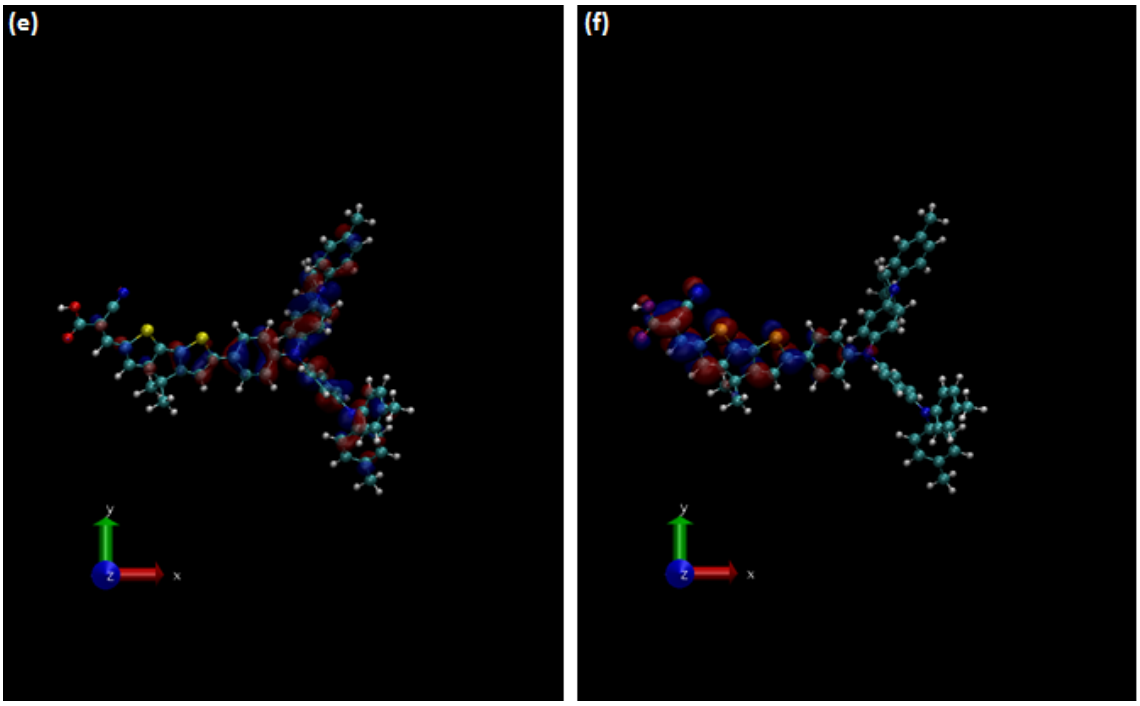

Figure S2. The HOMO of (a) D1, (c) D2, and (e) D3 and LUMO orbitals of (b) D1, (d) D2, and (f) D3

4. HOMO levels of 1, 2, and 3 measured by cyclic voltammetry

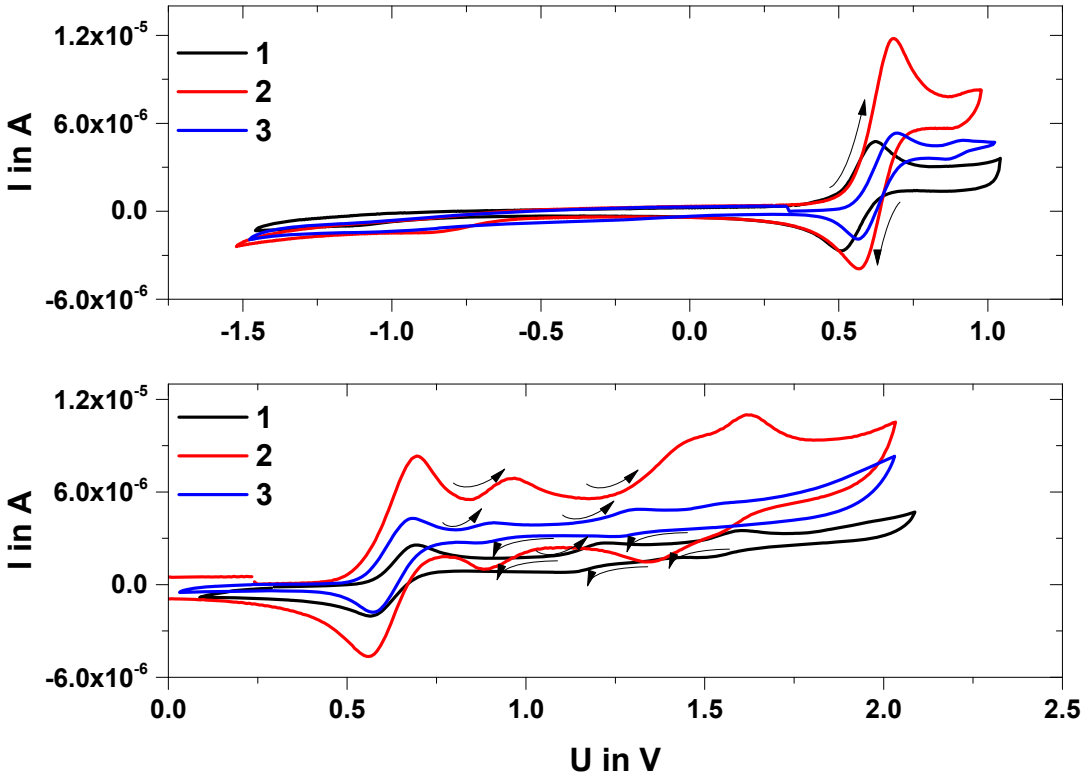

Figure S3. Cyclic voltammograms obtained on 0.1 M dichloromethane solution with an Ag/AgCl reference electrode and a platinum counter electrode (top: oxidation, bottom: reduction). The reference Fc/Fc^+ half wave potential was set to 0.6 V.

Cyclic voltammetry (CV) of **1-3** in dichloromethane with 0.1M $Bu_4N^+PF_6^-$ electrolyte was performed with an Ag/AgCl reference electrode and a platinum counter electrode giving reversible oxidation waves. No peaks were observed for the reduction likely due to the electron-rich nature of these compounds. The HOMO energies were calculated to -5.95 eV (**1**), -5.06 eV (**2**) and -5.10 eV (**3**). Thus, a difference in energy levels of approximately 1 eV for **1** to **2** and **3** was found.

5. Spiro-OMeTAD cation absorption graph using $FeCl_3$

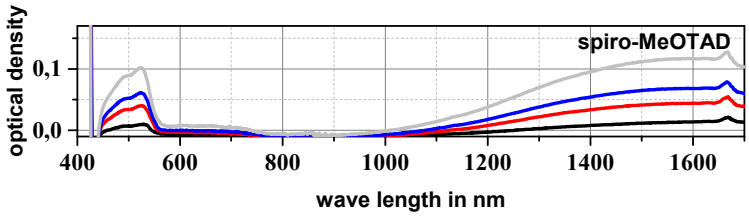

Figure S4. Steady-state absorption spectra of spiro-OMeTAD cations after addition of a 10 mM $FeCl_3$ solution.

Figure S4 shows the steady-state absorption of a 0.12 M spiro-OMeTAD solution in chlorobenzene (CB) after addition of 10 mM $FeCl_3$ in TLN. The absorption of cations is pronounced in three spectral regions between 440 – 550 nm, 550 – 760 nm, and 950 – 1650 nm and beyond, while the strongest absorption is observed in the near infrared, peaking at 1625 nm. Black, red, blue, and gray lines present 0.12 M spiro-OMeTAD mixed with 2, 5, 10, and 20 vl % of 10 mM $FeCl_3$ solution in CB, respectively. The absorption spectra of dye cations and spiro cations can be used as a fingerprint of injection and regeneration processes in photoinduced absorption experiment.

6. Injection efficiency (IE) calculation

Figure 3 panel (a) in the manuscript shows the PL intensity of dyes on a Al_2O_3 surface (solid lines, no injection) compared to a TiO_2 surface (dotted lines, injection possible), which provides an estimate of how efficiently the dye can inject electrons into TiO_2 by integrating each graph. The integration of each dye's PL intensity is summarized in the Table shown below. **1**, **2**, and **3** exhibit injection efficiencies of 92% (92% = (1 – 35605/442174)*100), 81 % (81 % = (1 – 199306/1023354)*100), and 97 % (97 % = (1 – 21989/889709)*100), respectively.

Table S2. The integrated PL intensity of dyes on film surfaces.

PL Intensity	**1**	**2**	**3**
On Al_2O_3	442174	1023354	889709
On TiO_2	35605	199306	21989
Li-treated TiO_2	5934	10688	117371

7. Effect of Li cations on 1 (charge generation)

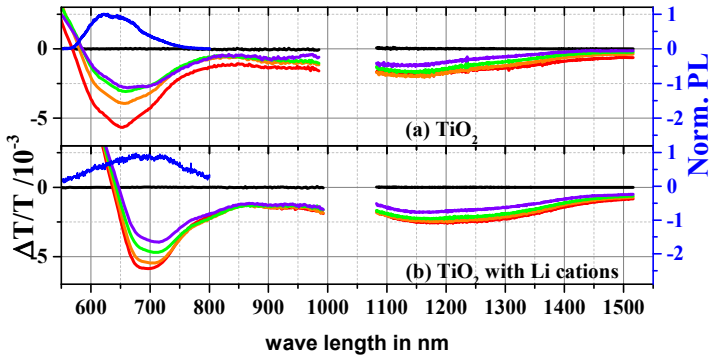

Figure S5. Short delay (ps-ns) broadband TA spectra of **1** on TiO_2 (a) and of **1** on TiO_2 after application of Li cations (b) at delay times of 3 ps (red), 30 ps (orange), 300 ps (green), and 3 ns (purple). The pump fluence at 520 nm is 5.5 µJ cm^{-2} for the visible and 7.0 µJ cm^{-2} for the near infrared measurements. The two blue lines represent the PL spectra of each sample.

In panel (a), the transient pump-probe spectra of **1** adsorbed on TiO_2 show two distinct features: positive TA signals up to 585 nm and negative TA signals extending to the near-infrared wavelength range. The positive and negative signals are assigned to ground state bleach (GSB) and photoinduced absorption (PIA) of excitons and dye cations. The long-lived negative PIA around 900 nm is not influenced by either the Stark effect or the PL spectrum; therefore, this wavelength region is assigned solely to dye cation absorption. Furthermore, these long-lived signals in the visible and NIR are not observed from **1** adsorbed on Al_2O_3, where we can observe only excitons including intra, inter, and interfacial charge transfer states. Therefore, the absorption of excitons and dye cations are observed in between 650-700 nm and between 800-1000 nm, respectively, and detection of long-lived dye cations implies that **1** is able to inject electrons without the help of Li-salt additives.

In panel (b), the transient absorption spectra of **1** after addition of Li cations are shown. They show clear evidence of long-lived charge generation. The amplitude of the charge absorption signal is stronger and most of the signal between 800-1000 and between 1150-1200 nm remains even after 3 ns. This is explained by enhanced absorption resulting from increased charge generation and decreased back electron transfer due to fast injection by the aid of Li cations. However, the spectrum at later times in panel (b) reflects the existence of dye cations as well as the decay of electrons in TiO_2 nanoparticles, because the strong peak between 650 – 750 nm looks still similar to the transient absorption spectrum in panel (a). These peaks red-shift due to a Stark effect that interferes with the ground state bleach of the dye molecules after insertion of Li cations.

8. Effect of Li cations on 2 (charge generation)

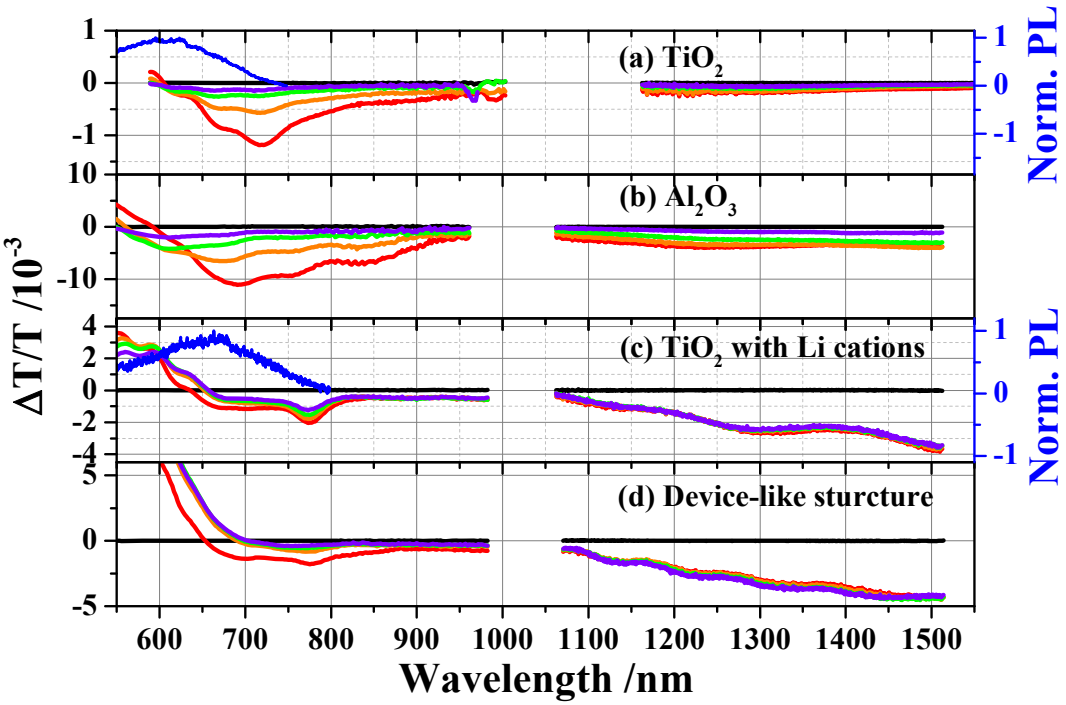

Figure S6. TA spectra on the femto- to nanosecond timescale and PL spectra of **2** on TiO_2 (a), of **2** on Al_2O_3 (b), and of **2** on TiO_2 after addition of Li cations (c) at delay time of 3 ps (red), 30 ps (orange), 300 ps (green), and 3000 ps (purple). The pump fluence at 510 nm is 5.5 µJ cm^{-2} in the visible and 7.0 µJ cm^{-2} in the NIR.

The figure above compares the visible and NIR pump-probe spectra between 3 ps and 3 ns of **2** adsorbed on TiO_2 with different additives, and shows the PL spectra. Panel (a) shows the TA spectra of **2** adsorbed on TiO_2 without any additive. The GSB signal extends to 600 nm and the broad negative PIA signals extend to the NIR. Most signals decay within 3 ns in the visible and NIR spectral range and there is no clear evidence that injection takes place in this sample. The reason can be found from the spectral shape and the fluence dependent measurements. When the spectral shape of panel (a) is compared to that of **2** on Al_2O_3 (panel b) and **2** on TiO_2 with Li cations (panel c), it appears more like the spectral shape of **2** on Al_2O_3 showing mainly exciton absorption. Hence, **2** on TiO_2 seems to show the absorption of excitons, rather than the absorption of dye cations.

Upon addition of Li cations as shown in panel (c), the TA spectra of **2** show two pronounced absorption features: a strong absorption around 780 nm and an increasing absorption peak in the NIR. These two features are assigned to the generation of dye cations by electron injection with the aid of Li cations. This was confirmed by quasi-steady-state PIA measurements on the same sample that showed a similar PIA spectrum as the TAS at 3 ps. Therefore, the injection seems to take place on an ultrafast timescale. Hence, exciton-induced absorption is likely absent due to fast injection in that the spectral shape of panel (c) looks quite different from the spectra in panel (a) and (b). Interestingly, the signals are fairly long-lived even beyond 3 - 4 ns, which supports a favorable injection process in **2** with the use of Li cations as is expected from the IE measurements, showing a large change in the number of the emitted photons upon the addition of Li cations.

9. Effect of Li cations on 3 (charge generation)

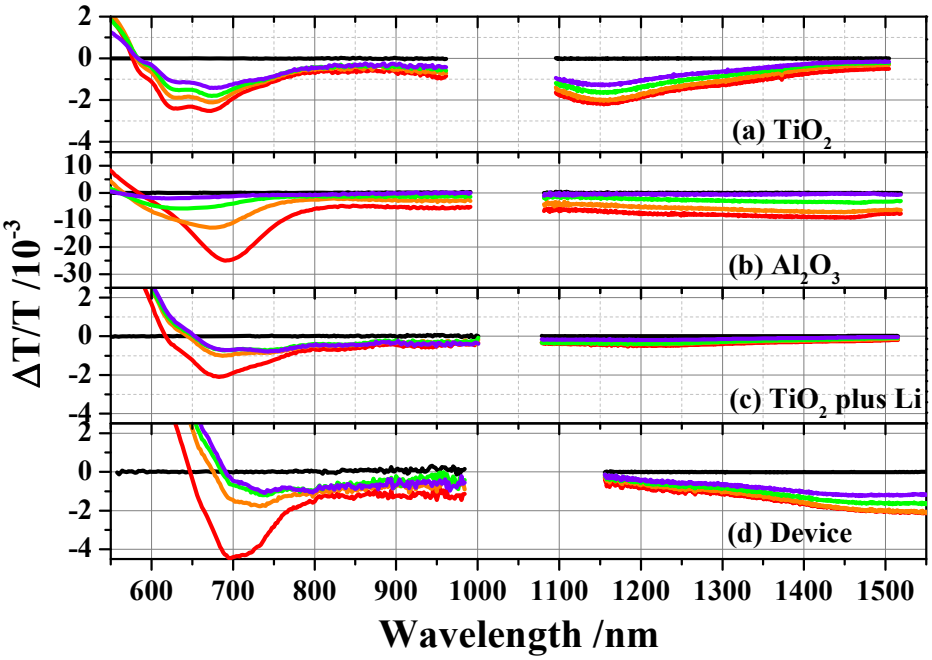

Figure S7.1. TA spectra on the femto- to nano-second timescale of FPH231 on TiO_2 (a), of FPH231 on Al_2O_3 (b), of FPH231 on TiO_2 with Li cations (c), and of the FPH231 device-like structure sample (d) at delay times of 3 ps (red), 30 ps (orange), 300 ps (green), and 3000 ps (purple). The pump fluence at 510 nm is 5.5 µJ cm^{-2} in the visible and 7.0 µJ cm^{-2} in the NIR.

Panel (a) in Figure S6 shows the transient absorption spectra of **3** adsorbed on TiO_2. The positive GSB signals are seen up to 580 nm and the negative PIA signals extend up to 1500 nm. The broad negative PIA signals are assigned to the dye cations formed due to electron injection even without the help of Li cations, since the spectral shape, especially in the NIR, is fairly similar to that in **3** on TiO_2 with Li cations in panel (c) rather than that in **3** on Al_2O_3 in panel (b). Panel (b) shows the short-time delay TA spectra of **3** on Al_2O_3, where we can mainly observe the absorption of the exciton and intramolecular charge transfer state when the dye molecule is adsorbed on the film. In panel (b), strong absorption peaks are observed between 650 – 700 nm and most signals decay in 300 - 1200 ps over the whole spectral range, whereas 30 % of the signal remains in panel (a) due to long-lived species. The assignment of the long-lived signals to charges is confirmed by the fluence dependence of long-time delay measurements shown in Figure S6.2.

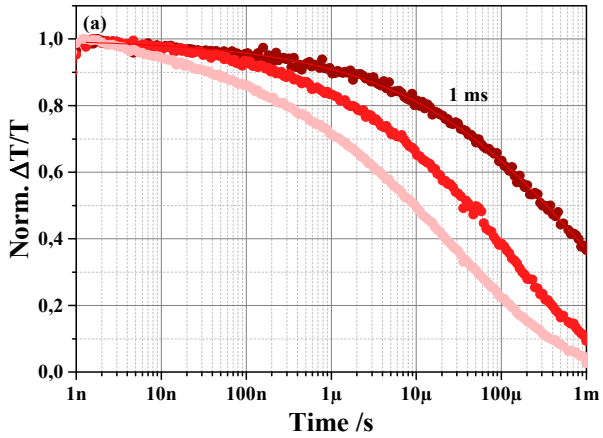

Figure S7.2. Transient absorption of dye cations between 1120 – 1150 nm in **3** on TiO_2 with Li cations.

In panel (c) of Figure S6.1, the transient absorption spectra of **3** after addition of Li salt are shown. Unlike **1** and **2**, the amplitude of the TA spectra decreases upon the use of Li cations, indicating less charge generation in line with the injection efficiency found in **3** on TiO_2 without Li cations. Furthermore, Figure S6.3. below shows the changes in the kinetics of **3** with (dark red) and without (light red) Li cations. The two samples exhibit rather similar decay kinetics indicating that Li cations do not significantly facilitate the charge generation like in **1** and **2**.

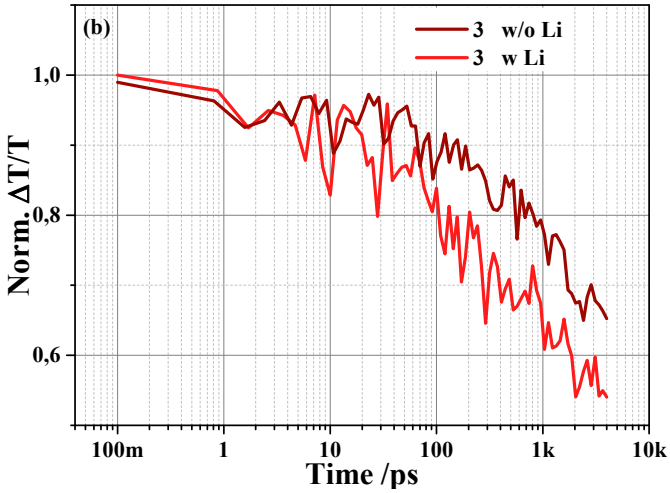

Figure S7.3. Kinetics of the dye cations in **3** on TiO_2 (red, 1150 – 1170 nm) and in **3** on TiO_2 with Li (dark red, 1120 – 1150 nm).

10. Absorption and emission spectra

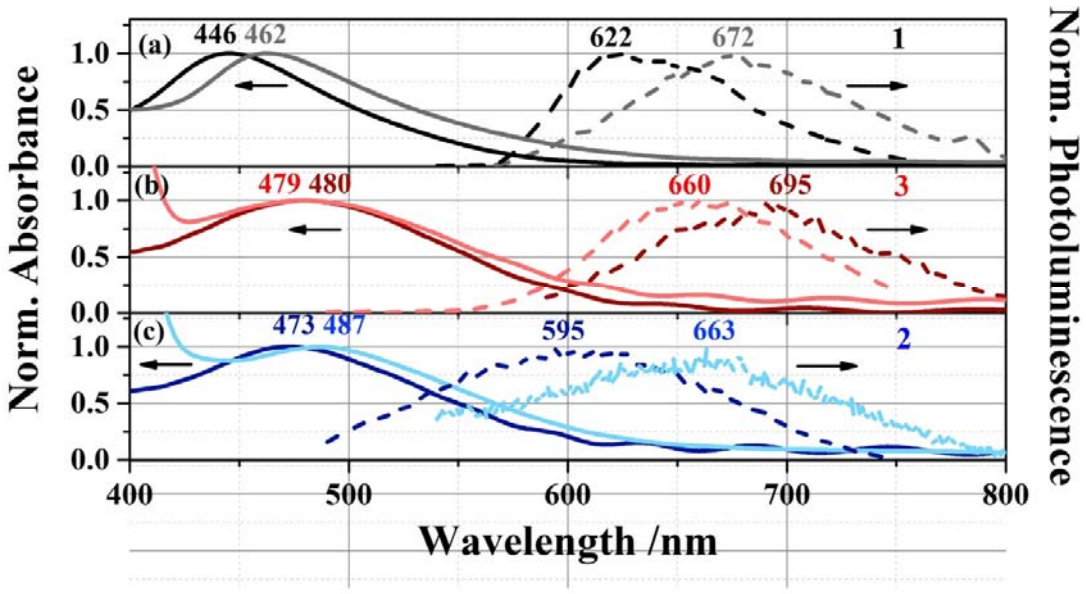

Figure S8. Normalized absorption and emission spectra of **1** (panel a), **3** (panel b), and **2**(panel c) adsorbed on titania in the presence (black, red, and blue) and absence (gray, pink, and sky blue) of Li cations.

Figure 7 shows normalized absorption and emission spectra of 3 dye molecules adsorbed on a TiO_2 surface in the absence (black, red, and blue) and absence (gray, pink, and sky blue) of Li cations. When the Li-TFSI salt is employed in films, D1 and D2 show a larger Stokes shift as shown in panel (a) and (c), respectively. This indicates that these dye molecules have a larger dipole moment in the excited state than in the ground state, leading to a more favorable injection process. D1 and D2 show similar Stokes shifts, but the absorption and emission spectra of D3 red-shift further compared to D1.

Red-shifted absorption and emission spectra after application of Li cations are related to the Stark effect that causes shifts of the energy levels of the dye. Injected electrons can induce local electric fields, and the orientation of the induced electric field and the dipole moment of the dye molecules determine the shift of absorption/emission spectra depending on their directions. Therefore, shifted absorption and emission spectra provide information about the dipole moment.

The absorption and emission spectra of D3 blue-shift with the addition of Li cations due to a more stabilized dipole moment in the ground state than in the excited state: from 480 nm to 479 nm in absorption spectra and from 695 nm to 660 nm in emission spectra. This is because Li cations create similar conditions to the excited state by creating a polar environment around the dye molecules.

11. TAS dynamics on the ps-ms time domain

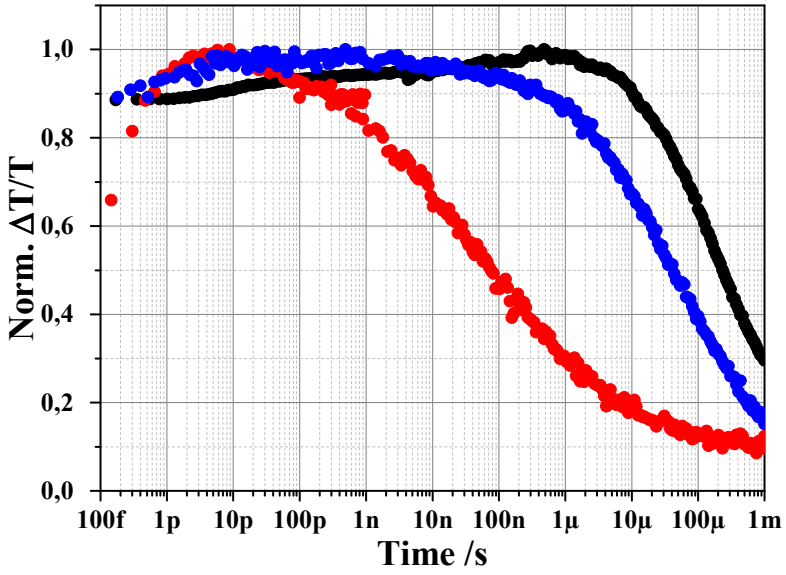

Figure S9. Transient absorption kinetics of spiro cation-induced absorption in the solar cell-like samples.

The figure above shows the ps – ms dynamics of oxidized spiro-OMeTAD molecules of the three samples. In the solar cell-like samples, **1** and **2** exhibit a slightly increasing or constant signal up to 1 ns – 1 µs, whereas **3** shows rising signals only up to 10 – 100 ps. For **3** fast increasing signals are observed due to reductive quenching, since both dyes showed remaining exciton signals from the TA spectra and the small PIA signals of the dye cations even after Li cations were used.